Remote Sensing, Yield, Physical Characteristics, and Fruit Composition Variability in Cabernet Sauvignon Vineyards

Brent Sams,[1,2]* Robert G.V. Bramley,[3] Luis Sanchez,[2] Nick Dokoozlian,[2] Christopher Ford,[1] and Vinay Pagay[1]

Abstract: Soil texture, topographical data, fruit zone light measurements, yield components, and fruit composition data were taken from 125 locations in each of four *Vitis vinifera* L. cv. Cabernet Sauvignon vineyards in the Lodi region of California during the 2017, 2018, and 2019 seasons. Data were compared against three sources of normalized difference vegetation index (NDVI) with different spatial resolutions: Landsat 8 ($LS8_{NDVI}$; 30 m), Sentinel-2 ($S2_{NDVI}$; 10 m), and manned aircraft (at high resolution, HR) with the interrow removed (HR_{NDVI}; 20 cm). The manned aircraft also captured canopy temperature (CT) derived from infrared (thermal) wavelengths (HR_{CT}; 40 cm) for additional comparisons. HR_{NDVI} was inversely related to HR_{CT}, as well as to several chemical components of fruit composition including tannins and anthocyanins. While some constituents of fruit composition such as anthocyanins may be related to NDVI, canopy temperature, and/or indirect measurements collected in the field, results presented here suggest that yield and fruit composition have a strong seasonal response and therefore environmental conditions should be considered if more accurate predictions are desired. Furthermore, freely available public satellite data sources with mixed canopy and interrow pixels, such as Sentinel-2 and Landsat 8, provided similar information related to predicting specific fruit composition parameters compared to higher resolution imagery from contracted manned aircraft, from which the interrow signal was removed. Growers and wineries interested in predicting fruit composition that accounts for spatial variability may be able to conserve resources by using publicly available imagery sources and small numbers of targeted samples to achieve this goal.

Key words: objective measures of fruit quality, precision viticulture, principal components analysis, remote sensing of vegetation, vineyard variability, *Vitis vinifera* cv. Cabernet Sauvignon

The prediction of winegrape composition in a vineyard, and the resulting wine quality, is difficult for numerous reasons. Manual sampling of fruit quality in vineyards can be complicated and time consuming (Wolpert and Vilas 1992, Meyers et al. 2011), especially for operations comprising many vineyards or many differentiated products. Additionally, comprehensive measures of fruit composition are expensive, requiring either costly commercial lab submissions, or in-house laboratory equipment and personnel. Furthermore, spatial variability exacerbates both of these issues because patterns of variability have shown to be temporally consistent but the magnitude of variability of fruit composition from a vineyard is unlikely to be consistent (Bramley 2005, Arnó et al. 2012, Sams et al. 2022).

Individual destructive vine measurements have long been the industry standard for determining fruit composition and potential wine quality. Commonly used vine measurements to evaluate vineyard performance are berry sizes or mass (Gladstones 1992), total yield estimates (Keller et al. 2005), dormant season pruning weights (Smart and Robinson 1991), and chemical analysis of berries or whole clusters (Niimi et al. 2020). More recently, to describe within-vineyard zones of potentially similar vine performance with a few targeted samples, indirect measurements like apparent electrical conductivity (EC_a) mapping have been shown to be useful in describing soil variability and its relationship with vine performance (Acevedo-Opazo et al. 2008, Bramley et al. 2011). Each of these measurements has an economic cost to vineyard managers and/or wineries, and few commercial operations collect sufficient samples to adequately characterize the full range of variability in a vineyard or have dedicated staff for time consuming surveys that are susceptible to changes in the environment or management practices over time (Ferreira et al. 2020).

Remote sensing can capture information on vineyard variability rapidly and repeatedly, but must be "ground-truthed,"

[1]School of Agriculture, Food, and Wine, Waite Research Institute, University of Adelaide, PMB 1, Glen Osmond, SA 5064, Australia; [2]Department of Winegrowing Research, E&J Gallo Winery, Modesto, California, USA; [3]CSIRO, Waite Campus, Locked Bag 2, Glen Osmond, SA 5064, Australia.

*Corresponding author (brent.sams@ejgallo.com)

Acknowledgments/Author disclosures: This work was funded by E. & J. Gallo Winery, CSIRO, and The University of Adelaide. The authors would like to thank the Winegrowing Research staff at E. & J. Gallo Winery for their help and support in the collection, processing, and analysis of the collected grape samples. The authors declare no conflicts of interest in the publication of this work.

Manuscript submitted Sept 2021, revised Nov 2021, Nov 2021, Nov 2021, accepted Dec 2021

doi: 10.5344/ajev.2021.21038

or validated by measurements collected at the field level, for crop metrics to be useful (Sun et al. 2017), although targeting indirect measurements or samples to vineyard zones based on spatial variability can reduce sample requirements (Meyers et al. 2011). Because all available sources of remote sensing information must be validated by ground measurements, and high-resolution imagery captured by many commercial manned aircraft platforms requires additional spectral and geometric calibrations for quantitative assessment, it would be useful to understand the capabilities of different sensors in predicting fruit composition at harvest to reduce these costs. As imagery from highly calibrated public satellite platforms like the European Space Agency's (ESA) Sentinel and the National Aeronautics and Space Administration's (NASA) Landsat becomes available at increasing spatial and temporal resolution, and at no cost, imagery obtained from manned and unmanned commercial aircraft flying at relatively low altitudes may not be necessary for many applications, such as discriminating zones for differential harvests or zonal vineyard management.

Remote sensing analysis of vineyards began in earnest two decades ago as Dobrowski et al. (2002) used imagery acquired using manned aircraft, and Johnson (2003) used imagery from satellites as tools for understanding grapevine canopies. Lamb et al. (2004), Bramley et al. (2011), Hall et al. (2011), Trought and Bramley (2011), and Song et al. (2014) found relationships between canopy vigor and fruit composition using normalized difference vegetation index (NDVI) and plant cell density derived from imagery acquired from manned aircraft, while Sun et al. (2017) used Landsat-derived products (NDVI and leaf area index) to predict winegrape yield. Sozzi et al. (2020) showed significant relationships in vineyard canopy variability (NDVI) captured by Sentinel-2 versus high-resolution imagery from an unmanned aerial vehicle (UAV), with comparisons of interrow removed and included, but they did not relate these to measurements of yield or fruit composition. Given these findings, and the fact that several compounds found in Cabernet Sauvignon grapes known to influence wine chemistry are related to environmental conditions (Bergqvist et al. 2001, Kliewer and Dokoozlian 2005, Lee et al. 2007, Li et al. 2013, Martínez-Lüscher et al. 2019), we hypothesize that it should be possible to characterize the relationships among vine productivity, seasonal growing conditions, and remote sensing. Principal component analysis (PCA), a method commonly used to reduce dimensionality of large data sets, has been used by others to infer relationships between some aspects of yield and fruit composition with soil variables in Chardonnay in Ontario, Canada (Reynolds et al. 2013), and imagery, water status, soil characteristics, basic grape chemistry, and yield of different varieties in France (Acevedo-Opazo et al. 2008).

We present results of PCA and Pearson correlations combining data from four commercial vineyards in the Lodi region of California with different management strategies, terrains, soil types, and magnitudes of variability. Our objectives were to compare variables from different remote sensing sources with a large volume of spatially distributed and ground-truthed environmental and fruit composition measurements, as well as to determine the most useful and efficient ground-truthing descriptors of vineyard characteristics correlating to fruit composition and quality. To our knowledge, no study exists incorporating yield components, fruit chemistry, soil texture, fruit zone light, and remote sensing with high density ground validation. Additionally, the inclusion of Cabernet Sauvignon grape mouthfeel and aroma precursors differentiates the present analysis from previous studies relying mainly on measures of basic chemistry.

Materials and Methods

Four Cabernet Sauvignon vineyards were selected based on their range of geographic locations and assessments of spatial variability found in aerial imagery and were sampled for yield components and fruit composition at harvest for three consecutive seasons, 2017 to 2019 (Sams et al. 2022). The vineyards were in the American Viticultural Area (AVA) of Lodi, California and were within 40 km of one another and spatially distributed across the AVA. Climate of the region is classified as dry summer subtropical with an average of 190 mm of precipitation annually. Summertime highs regularly exceed 40°C and winter lows rarely dip below 0°C. Climate data were summarized from a centrally located weather station in the Lodi region for the three years in which data were collected (Table 1). Table 2 details the physical characteristics of each vineyard. Briefly, all four vineyards—Vineyards A through D—were drip irrigated and had sprawling, spur-pruned canopies. Vineyard C was planted in 1998, while Vineyards A, B, and D were planted from 2010 to 2013.

Yield and fruit composition. On the commercial harvest dates for each of the four vineyards set by the receiving winery in each season, a three-step process for documenting yield components was completed at each of the spatially distributed 125 georeferenced data vines in each vineyard. Sample distribution maps can be found in Sams et al. (2022). A combined 100-berry sample was collected by randomly selecting 10 clusters and removing 10 total berries from the top, middle, and bottom of each cluster and weighed. Twenty randomly chosen grape clusters were then removed from each data vine, weighed, and transported to the laboratory. Data vines were hand-harvested and total yield per vine and cluster number were recorded. Weights from all three steps were combined for total vine yield. Upon arrival at the laboratory, all berries from the 20 randomly chosen grape clusters were homogenized before extraction with acidified 50% ethanolic solution. Total anthocyanins were measured using a UV-vis based method described by Iland et al. (2000). Polymeric tannins and a combined total of quercetin 3-*O*-glucoside and 3-*O*-glucuronide, referred to hereafter as "quercetin glycosides," were measured using reversed-phase high-performance liquid chromatography (HPLC; Peng et al. 2001). Analysis of free-form volatile compounds (C6 and 3-isobutyl-2-methoxypyrazine [IBMP]) was completed using headspace solid-phase microextraction coupled to a gas chromatograph

and a mass spectrometer (HS-SPME-GC-MS) adapted from Kotseridis et al. (2008) and Canuti et al. (2009). Bound form β-damascenone was extracted using solid phase extraction adapted from Whiton and Zoecklein (2002), followed by fast acid hydrolysis and SPME-GC-MS as described by Kotseridis et al. (1999), Ibarz et al. (2006), and Canuti et al. (2009). Total soluble solids (Brix), pH, titratable acidity (TA), yeast assimilable nitrogen (YAN), and malic acid were measured using standard methods of Fourier-transform infrared spectroscopy and calibrated using E. & J. Gallo's reference chemistry standards.

Vineyard physical characteristics. Soil cores were collected between seasons (Vineyards B and C in December 2018; Vineyards A and D in December 2019) from the center of the interrow space ~1 m from each data vine using a 5.7 cm diam soil auger (AMS, Inc.). Each core constituted a single composite sample of soil depths from 0 to 100 cm taken at 20 cm increments, mixed into a 30.5 × 25.4 cm plastic bag, and submitted to a commercial soil analysis laboratory (A & L Western Laboratories) for particle size (texture) analysis. An apparent EC_a survey was conducted in each vineyard prior to the initiation of vine growth in 2018 using a Dualem-1S (Dualem Inc.) and a Trimble Geo7x Global Positioning System (GPS, Trimble Inc.). EC_a data were interpolated in VESPER using local block kriging (version 1.62; Australian Centre for Precision Agriculture, The University of Sydney, New South Wales, Australia). A digital elevation model developed from a range of sources and with a final resolution of ~10 m ground spacing (1/3 arc-second) and a vertical root mean square error of 1.55 m (Gesch et al. 2014) was downloaded from the United States Geological Survey (USGS) and used for topographic analysis (USGS 2019, 3D Elevation Program Digital Elevation Model, accessed 21 March 2020 at https://elevation.nationalmap.gov/arcgis/rest/services/3DEPElevation/ImageServer).

Measurements of photosynthetically active radiation (PAR) in the fruit zone of each data vine were collected in the first week of June in 2018 and 2019 at bloom (modified Eichhorn-Lorenz [E-L] stage 23; Pearce and Coombe 2004), mid-June or fruit set (modified E-L stage 27), and mid-July or veraison (modified E-L stage 35), with measurements occurring only on days with relatively cloudless sky conditions. PAR measurements were taken within two hours of solar noon using an ACCUPAR LP-80 ceptometer (Meter Group, Inc.). In the two bilateral cordon trained vineyards (Vineyards A and D), the ceptometer was placed parallel to the vine cordons in the fruiting zones of the canopies and facing up and on both the north and south sides of the vines, with one above canopy (or ambient) measurement taken before and one after the fruit zone measurements. In the two horizontally divided quadrilateral-cordon trained vineyards (Vineyards B and C), one measurement was taken on the south side of each southern cordon and one measurement on the north side of each northern cordon, with ambient measurements taken before and after fruit zone measurements. The sensor console was aligned horizontally with the vine trunk in all vineyards, ensuring that the main arm from the trunk to the center of the vine was accounted for in each measurement. Measurements from each vine were averaged and fruit zone PAR (PAR_{FZ}) was calculated by dividing the average fruit zone PAR measurements by the average of the ambient PAR measurements. Additional ambient incident PAR measurements were taken in open areas with no overhead sensor obstruction every 15 min throughout each measurement period to ensure above canopy measurements reflected ambient conditions and were not obstructed by neighboring vine rows. Dormant season pruning weights were collected in the first two weeks of December in 2018 and 2019 from each data vine and the Ravaz index was calculated as the ratio of yield:pruning weight (Smart and Robinson 1991).

Table 1 Regional growing degree days, precipitation, radiation, and reference evapotranspiration (ET_o) by annual quarters from 2017 to 2019 in the Lodi region of California.

	Phenology	E-L[a]	Date ranges	Growing degree days ($Base_{10}$)	Precipitation (mm)	Radiation (W m^2)	ET_o (mm)
2017	Leaf fall-budbreak	[43-04]	Nov 2016-March	561	614	3095	282
	Budbreak-fruit set	[05-26]	April-May	476	47	2717	323
	Fruit set-veraison	[27-35]	June-July	690	2	3323	372
	Veraison-harvest	[36-42]	Aug-Oct	959	4	3827	392
			2017 Totals	**2686**	**667**	**12,962**	**1369**
2018	Leaf fall-budbreak	[43-04]	Nov 2017-March	548	298	3395	253
	Budbreak-fruit set	[05-26]	April-May	438	65	3000	279
	Fruit set-veraison	[27-35]	June-July	668	0	3412	372
	Veraison-harvest	[36-42]	Aug-Oct	881	1	3864	382
			2018 Totals	**2535**	**364**	**13,671**	**1286**
2019	Leaf fall-budbreak	[43-04]	Nov 2018-March	500	488	3112	238
	Budbreak-fruit set	[05-26]	April-May	439	67	2812	260
	Fruit set-veraison	[27-35]	June-July	682	0	3419	367
	Veraison-harvest	[36-42]	Aug-Oct	849	7	3628	372
			2019 Totals	**2470**	**562**	**12,971**	**1237**

[a]Modified Eichhorn-Lorenz (E-L) stages, Pearce and Coombe 2004. Source: Lodi Winegrape Commission Weather station network (https://lodi.westernweathergroup.com); Station ID: Valley Oak.

Remote sensing—manned aircraft. High-resolution imagery from manned aircraft (visible/near-infrared = 0.2 m ground resolution, wavelengths = 800, 670, 550 µm, bandwidth =10 nm; thermal infrared/canopy temperature = 0.4 m ground resolution, wavelengths = 7.5 to 13 µm; absolute error ±1°C) was sourced from a commercial provider for each vineyard at phenological stages corresponding to the PAR measurements in 2018 and 2019 (modified E-L stages 23, 27, 35). NDVI was calculated from the near-infrared (800 nm) and red (670 nm) bandwidths (Rouse et al. 1974). Using the histogram for each HR_{NDVI} and HR_{CT}, a bimodal separation of pixels was used to delineate canopy pixels from pixels in the interrow and nonvine signals (Salgadoe et al. 2019). All noncanopy pixels, or those below the histogram separation values in the case of NDVI and above the histogram separation values in the case of thermal infrared, were removed, and the average pixel value of each data vine was derived from the remaining pixels. Image processing was completed using ArcGIS (v10.4, Environmental Systems Research Institute).

Remote sensing—satellites. Sentinel-2 (10-m pixel) and Landsat 8 (30-m pixel) satellite images were processed and downloaded using the Google Earth Engine (Gorelick et al. 2017). Level-1 precision- and terrain-corrected Landsat 8 images were atmospherically corrected to surface reflectance prior to retrieval (Vermote et al. 2016). Because of a lack of available surface reflectance imagery for the study area in 2018, top of atmosphere images from Sentinel-2 were used to maintain a consistent source. Images from satellite overpasses corresponded to acquisition dates closest to PAR measurements and relatively cloudless dates to compare results of each source with phenological stages. NDVI ($S2_{NDVI}$ and $LS8_{NDVI}$) was calculated for each image using each sensor's respective near-infrared (NIR; LS8 = 851 to 879 nm, S2 = 785 to 899 nm) and red (LS8 = 636 to 679 nm, S2 = 650 to 680 nm) bands. Data points corresponding to pixels with more than 20% of each pixel's area outside of each vineyard, i.e., edge pixels, were not included in subsequent analyses.

PCA. PCA was conducted in R statistical software (R Core Team 2020, R Foundation for Statistical Computing, https://www.R-project.org/) using the FactoMineR package (Lê et al. 2008). Because berry weights, cluster counts, and pruning weights were not recorded in 2017, the 2017 data were not included in the further analyses, which used complete data sets for 2018 and 2019. All fruit compositional data, yield components, images, and environmental measurements were standardized by vineyard and season (mean = 0, standard deviation = 1) to eliminate site specific, vintage, and management effects (Carrillo et al. 2016). A modified *t*-test that accounted for spatial autocorrelation (Dutilleul 1993) was calculated using the SpatialPack package in R (Vallejos et al. 2020) to assess the strength of the relationships among the characteristics of the fruit, yield components, soil, topography, and imagery.

Table 2 Physical details, cultural practices, vine characteristics, and irrigation rates applied in 2017 to 2019 in four vineyards in the Lodi region of California.

	Vineyard A	Vineyard B	Vineyard C	Vineyard D
Training method	Single bilateral	Quadrilateral	Quadrilateral	High wire
Trellis system	Sprawl	Sprawl	Sprawl	Sprawl
Vine spacing (m)	2.1	1.2	1.8	2.4
Row spacing (m)	3.1	3.4	3.4	3.1
Vineyard area (ha)	7.4	13.8	11.8	11.2
Sample density (per ha)	17.0	9.0	11.0	11.0
Year planted	2010	2013	1998	2012
Rootstock/ scion clone	039-16/ FPS08	SO4/7	1103P/7	039-16/15
Rootstock parentage	*Vitis vinifera* × *Vitis rotundifolia*	*Vitis berlandieri* × *Vitis riparia*	*V. berlandieri* × *Vitis rupestris*	*V. vinifera* × *V. rotundifolia*
Pruning method	Hand	Hand	Hand	Machine
Floor management	Tilled bare soil	Perennial cover crop	Perennial cover crop	Perennial cover crop
Elevation (min to max; m asl)	6.3 to 7.1	38.9 to 60.4	20.1 to 21.6	39.6 to 47.0
Applied irrigation (mm)				
2017	No data	401	219	No data
2018	No data	415	145	289
2019	No data	423	197	281

Results

Results from PCA when data were not standardized show that relationships between variables (descriptive statistics can be found in Table 3) were driven by site and seasonal effects (Figure 1A and 1B). However, combined standardized data in PCA from all four vineyards exhibited a typical global response as points from each vineyard and season overlapped and were distributed approximately evenly around the origin (Figure 1C and 1D). Figure 2 revealed similar relationships from the three sources of NDVI imagery (HR_{NDVI}, $S2_{NDVI}$, and $LS8_{NDVI}$), and inverse relationships with HR_{CT}. Imagery from three phenological stages were within ~3% of one another in terms of variance explained by PCA, although no single combination of component one (PC1) and component two (PC2) explained more than 40% of the multivariate variability (Figure 2). NDVI from all three sources of imagery was related to pruning weights, and the relationship strengthened as the seasons progressed. HR_{CT} separated with PAR_{FZ} at bloom and veraison (Figure 2). $LS8_{NDVI}$ showed the weakest relationships with fruit composition and vine performance

Table 3 Fruit composition, crop characteristics, and soil texture measured in 2017 to 2019 in four vineyards in the Lodi region of California.[a]

	Vineyard A			Vineyard B			Vineyard C			Vineyard D		
	2017	2018	2019	2017	2018	2019	2017	2018	2019	2017	2018	2019
Fruit composition												
Total soluble solids (Brix)	24.4 ± 0.5	24.4 ± 0.7	24.4 ± 0.8	24.8 ± 1.0	26.5 ± 0.8	25.4 ± 1.3	24.6 ± 0.9	25.4 ± 0.8	25.0 ± 1.2	24.3 ± 1.2	24.7 ± 1.4	25.3 ± 1.6
pH	3.78 ± 0.06	3.85 ± 0.06	3.87 ± 0.08	3.83 ± 0.07	3.79 ± 0.06	3.63 ± 0.07	3.88 ± 0.12	3.80 ± 0.10	3.73 ± 0.11	3.67 ± 0.14	3.60 ± 0.08	3.63 ± 0.10
Titratable acidity (g/L)	3.7 ± 0.3	3.8 ± 0.5	3.7 ± 0.3	3.2 ± 0.3	3.1 ± 0.3	3.1 ± 0.5	3.8 ± 0.5	3.4 ± 0.5	3.5 ± 0.6	3.8 ± 0.5	3w.8 ± 0.6	3.6 ± 0.5
Anthocyanins (mg/g)	0.79 ± 0.10	1.21 ± 0.19	0.72 ± 0.12	1.15 ± 0.19	2.19 ± 0.21	1.10 ± 0.11	1.34 ± 0.22	2.45 ± .38	1.30 ± 0.20	0.89 ± 0.16	1.89 ± 0.31	0.90 ± 0.14
β-damascenone (µg/g)	46 ± 5	60 ± 7	59 ± 6	59 ± 7	83 ± 12	60 ± 6	57 ± 6	79 ± 10	67 ± 8	48 ± 7	54 ± 7	49 ± 7
C6 (µg/g)	5.3 ± 0.5	5.0 ± 0.8	5.2 ± 0.8	4.2 ± 0.9	3.2 ± 0.6	4.1 ± 0.9	3.1 ± 0.7	3.2 ± 0.8	1.5 ± 0.7	5.2 ± 1.1	4.7 ± 1.1	1.6 ± 0.6
IBMP (pg/g)[b]	5.5 ± 3.3	3.8 ± 3.8	2.1 ± 3.0	0.2 ± 0.9	2.1 ± 2.8	ND[c]	0.1 ± 0.5	0.1 ± 0.7	ND	2.0 ± 2.0	ND	0.1 ± 0.5
Malic acid (g/L)	1.9 ± 0.3	2.2 ± 0.4	1.9 ± 0.3	1.3 ± 0.2	1.6 ± 0.3	0.9 ± 0.3	1.5 ± 0.4	1.7 ± 0.3	1.0 ± 0.5	1.6 ± 0.3	1.7 ± 0.3	1.1 ± 0.4
Polymeric tannins (mg/g)	2.0 ± 0.3	1.4 ± 0.2	1.8 ± 0.2	3.6 ± 0.8	2.2 ± 0.3	2.4 ± 0.3	3.2 ± 0.6	2.7 ± 0.4	3.6 ± 0.6	2.3 ± 0.5	2.2 ± 0.2	2.4 ± 0.5
Quercetin glycosides (µg/g)	35 ± 9	24 ± 7	29 ± 8	102 ± 31	25 ± 9	82 ± 19	59 ± 22	47 ± 18	79 ± 21	50 ± 16	46 ± 7	73 ± 25
YAN (g/L)[b]	0.15 ± 0.03	0.26 ± 0.03	0.17 ± 0.03	0.03 ± 0.01	0.09 ± 0.02	0.02 ± 0.02	0.05 ± 0.02	0.06 ± 0.02	0.04 ± 0.02	0.10 ± 0.03	0.07 ± 0.03	0.04 ± 0.02
Yield components												
Yield (kg/m^2)	2.6 ± 0.5	3.0 ± 0.5	3.1 ± 0.6	1.3 ± 0.4	2.1 ± 0.4	2.3 ± 0.6	1.7 ± 0.5	1.9 ± 0.6	1.6 ± 0.5	2.5 ± 0.6	2.8 ± 0.5	2.3 ± 0.6
Cluster weight (g)	NS[c]	173 ± 21	155 ± 16	NS	121 ± 17	101 ± 20	NS	92 ± 16	78 ± 16	NS	131 ± 20	105 ± 25
Clusters (count/m^2)	NS	18 ± 3	20 ± 5	NS	18 ± 3	23 ± 4	NS	20 ± 5	20 ± 5	NS	21 ± 3	22 ± 4
Berry weight (g)	NS	1.09 ± 0.08	1.18 ± 0.09	NS	1.13 ± 0.10	1.09 ± 0.10	NS	0.87 ± 0.12	0.95 ± 0.13	NS	1.16 ± 0.09	1.25 ± 0.12
Canopy measurements												
Pruning weight (kg/m^2)	NS	0.47 ± 0.08	0.28 ± 0.05	NS	0.19 ± 0.05	0.35 ± 0.07	NS	0.29 ± 0.09	0.24 ± 0.06	NS	0.26 ± 0.05	0.29 ± 0.07
Ravaz index (kg/m^2)	NS	6.5 ± 1.1	11.0 ± 2.4	NS	11.8 ± 2.9	6.9 ± 2.2	NS	6.7 ± 1.4	6.7 ± 1.9	NS	10.9 ± 2.2	8.0 ± 2.3
PAR_{FZ}[d] – E-L 23 (% ambient)	NS	0.6 ± 0.9	2.1 ± 2.1	NS	3.4 ± 2.3	4.5 ± 3.7	NS	9.6 ± 10.4	4.0 ± 2.7	NS	1.2 ± 1.1	1.1 ± 0.6
PAR_{FZ} – E-L 27 (% ambient)	NS	0.7 ± 0.6	1.2 ± 1.1	NS	1.8 ± 1.3	6.6 ± 3.9	NS	4.2 ± 6.3	3.9 ± 3.1	NS	1.2 ± 0.7	1.5 ± 1.4
PAR_{FZ} – E-L 35 (% ambient)	NS	1.6 ± 2.9	2.9 ± 2.9	NS	4.3 ± 2.4	9.5 ± 4.8	NS	10.1 ± 7.2	13.9 ± 8.3	NS	4.4 ± 3.8	7.6 ± 6.0
Soil measurements[e]												
Clay (%)		14 ± 2			26 ± 4			20 ± 6			15 ± 3	
Silt (%)		29 ± 6			28 ± 4			33 ± 9			24 ± 7	
Sand (%)		57 ± 7			45 ± 4			47 ± 12			61 ± 8	
EC_a[b] (mS/m^2)		96 ± 11			127 ± 19			88 ± 17			92 ± 13	

[a]Values are mean ± SD, n = 125.
[b]IBMP, 3-isobutyl-2-methoxypyrazine; YAN, yeast assimilable nitrogen; EC_a, apparent electrical conductivity.
[c]ND, not detected; NS, not sampled.
[d]PAR_{FZ} = fruit zone photosynthetically active radiation; modified Eichhorn-Lorenz (E-L) stages (Pearce and Coombe 2004).
[e]Soil data were collected in December 2018 at Vineyards B and C, and in December 2019 at Vineyards A and D.

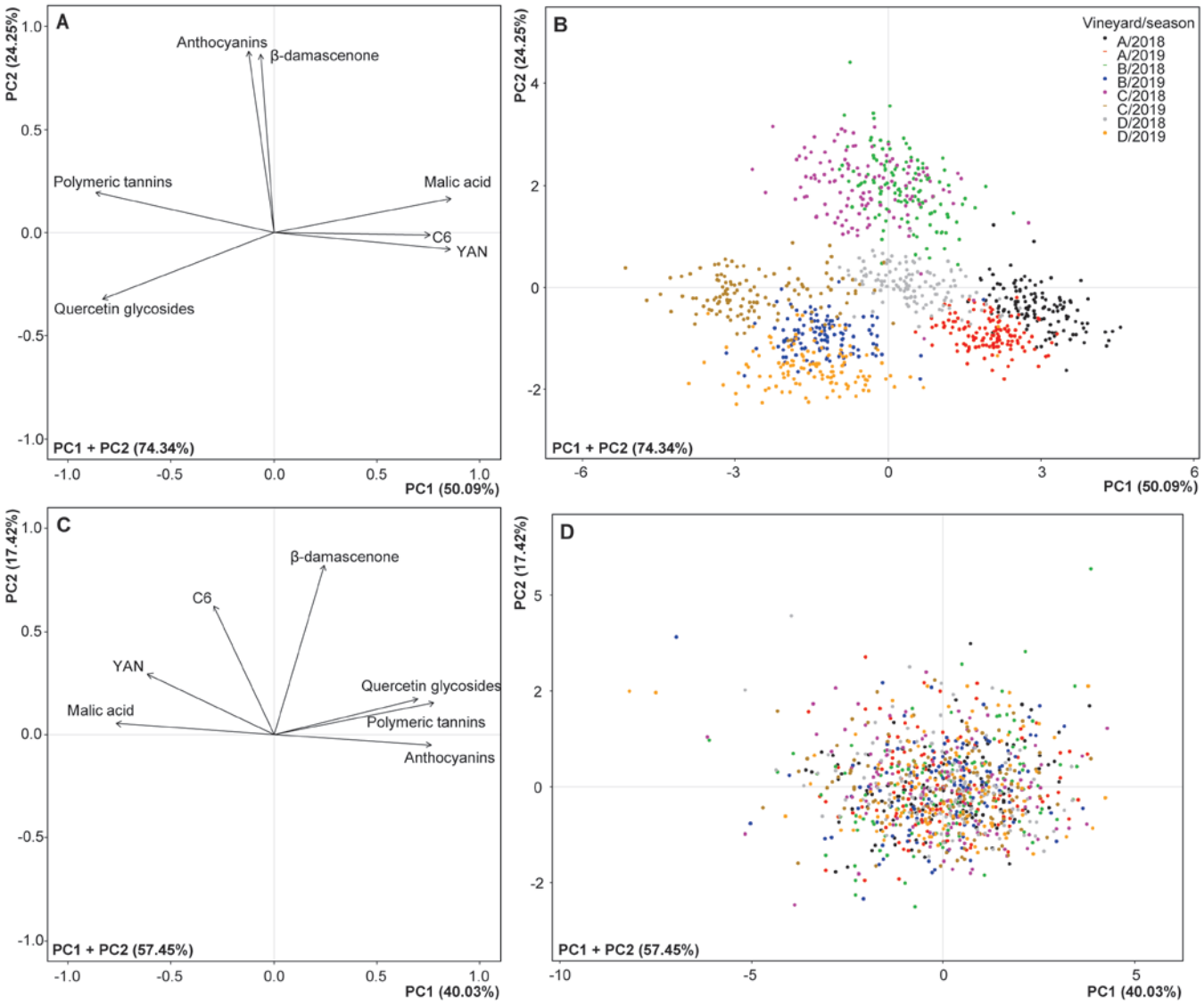

Figure 1 Principal component analysis (PCA) of fruit components (anthocyanins, β-damascenone, C6, malic acid, polymeric tannins, quercetin glycosides, and yeast assimilable nitrogen [YAN]) measured in four vineyards (A, B, C, and D) in the Lodi region of California in 2018 and 2019: (**A**) relationships among nonstandardized variables (loadings), (**B**) distribution of data points from each vineyard and season (scores), (**C**) relationships among standardized (μ = 0, σ = 1) variables (loadings), and (**D**) distribution of standardized (μ = 0, σ = 1) data points from each vineyard and season (scores). n = 1000 (125/vineyard/year).

variables, as evidenced by its limited distance from the center axis (Figure 2) and the weakest Pearson coefficients (Table 4). Visual comparisons of imagery captured at veraison (modified E-L stage 35) in Vineyard C highlight the similarities in the pattern of vigor captured by Landsat 8, Sentinel-2, and high-resolution NDVI, as well as the high-resolution canopy temperature (Figure 3). This similarity was apparent despite the removal of edge pixels in $S2_{NDVI}$ and $LS8_{NDVI}$ and the removal of interrow pixels in the HR_{CT} and HR_{NDVI}. Additionally, high values of HR_{CT} corresponded to low values of HR_{NDVI}, $S2_{NDVI}$, and $LS8_{NDVI}$ (Figure 3), and this visual relationship was mirrored by PCA (Figure 2) and correlation analysis (Table 4).

Quercetin glycosides, polymeric tannins, anthocyanins, and β-damascenone were grouped together and were positively related to HR_{CT} and inversely related to NDVI from all three sources (Figure 2 and Table 4). Malic acid, YAN, and C6 were typically related with low PAR_{FZ} and were closely related to pruning weights and yield, as well as NDVI in PC1 (Figure 2). Fruit yield per square meter and berry weight were relatively well spread along PC1 when compared with phenolic compounds, which were tightly grouped (Figure 2). While the results from PCA showed many of these variables to be closely related, results from the modified *t*-test showed that although many of these were significantly correlated ($p < 0.05$), the correlations for many were weak (Table 4). Correlations of fruit composition variables with yield components and pruning weights were generally strong, whereas correlations among most imagery, PAR_{FZ}, and topographic variables produced coefficients <0.2 (Table 4).

Figure 4 shows the relative positions among fruit composition, PAR_{FZ}, and yield components in each of the four

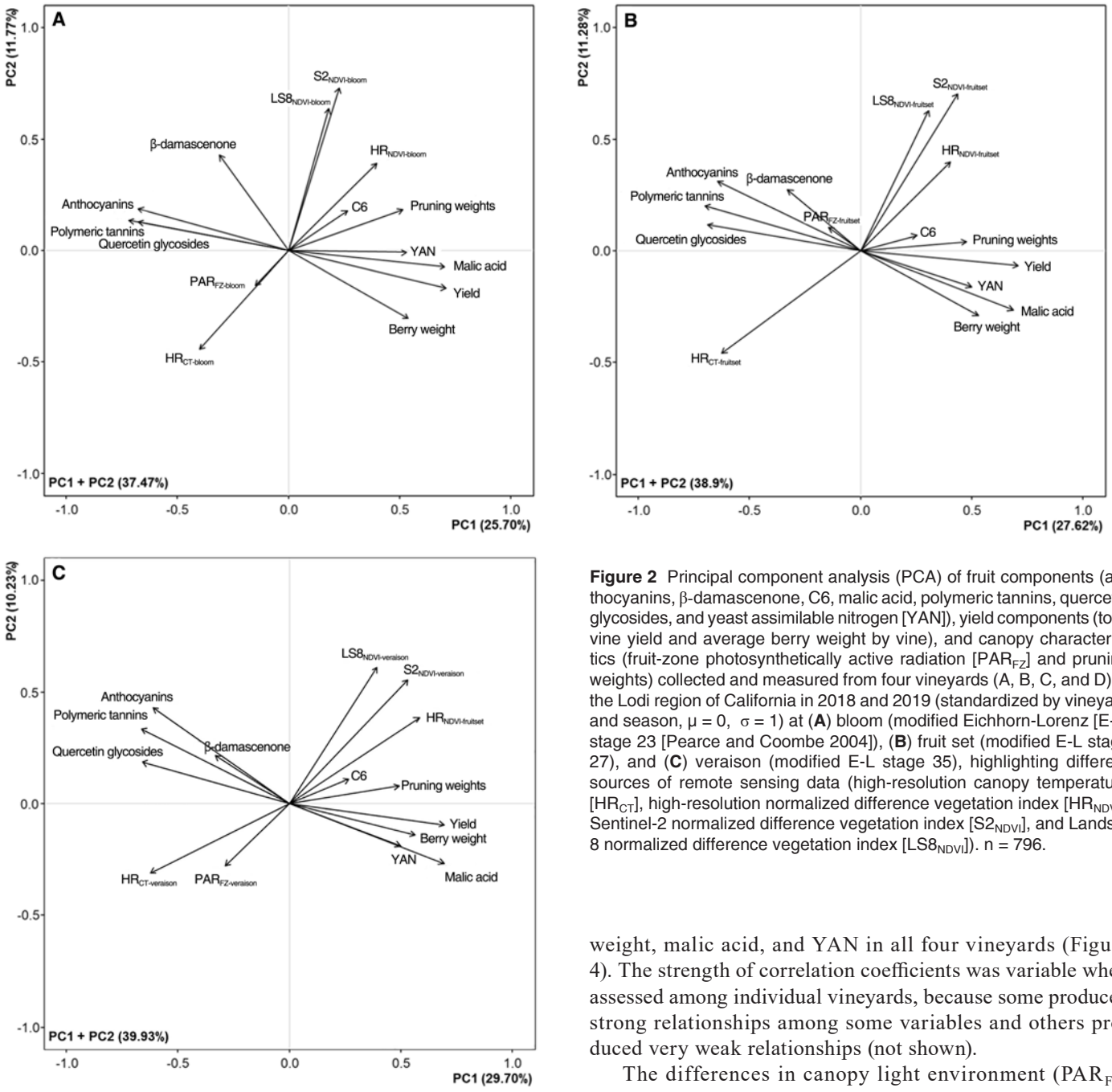

Figure 2 Principal component analysis (PCA) of fruit components (anthocyanins, β-damascenone, C6, malic acid, polymeric tannins, quercetin glycosides, and yeast assimilable nitrogen [YAN]), yield components (total vine yield and average berry weight by vine), and canopy characteristics (fruit-zone photosynthetically active radiation [PAR_{FZ}] and pruning weights) collected and measured from four vineyards (A, B, C, and D) in the Lodi region of California in 2018 and 2019 (standardized by vineyard and season, $\mu = 0$, $\sigma = 1$) at (**A**) bloom (modified Eichhorn-Lorenz [E-L] stage 23 [Pearce and Coombe 2004]), (**B**) fruit set (modified E-L stage 27), and (**C**) veraison (modified E-L stage 35), highlighting different sources of remote sensing data (high-resolution canopy temperature [HR_{CT}], high-resolution normalized difference vegetation index [HR_{NDVI}], Sentinel-2 normalized difference vegetation index [$S2_{NDVI}$], and Landsat 8 normalized difference vegetation index [$LS8_{NDVI}$]). n = 796.

vineyards. Vineyards had different mean values and magnitudes of variation in some variables (Table 3). Relationships among fruit compositional variables were similar in all vineyards, specifically along the first principal component (Figure 4). Groups of phenolic compounds (polymeric tannins, quercetin glycosides) segregated on the opposite side of several compounds related to shaded or unripe fruit (C6, malic acid). Larger yields, berry weights, and pruning weights also aligned more closely with characteristics of unripe fruit in all four vineyards (Figure 4). Similar to the relationship when all four vineyards were combined (Table 4 and Figure 2), PAR_{FZ} was positively related to phenolic compounds and inversely related to pruning weights, yield per meter, berry weight, malic acid, and YAN in all four vineyards (Figure 4). The strength of correlation coefficients was variable when assessed among individual vineyards, because some produced strong relationships among some variables and others produced very weak relationships (not shown).

The differences in canopy light environment (PAR_{FZ}) from fruit set (modified E-L stage 23) to veraison (modified E-L stage 35) shows that fruit in Vineyard A received less than 1% of ambient PAR compared with up to nearly 10% during this period in the other vineyards (Table 3). Vineyard D was only slightly more exposed than Vineyard A in the first two measured modified E-L stages (stage 23–bloom, and stage 27–fruit set), but because of canopy management practices, this percentage increased by veraison to levels similar to those observed in Vineyards B and C where fruit color was much higher. PAR_{FZ} was more variable in Vineyards B and C compared with Vineyards A and D, and generally matched the results of anthocyanins and several other variables (Table 3). Soil variables (sand, silt, clay, EC_a) were sometimes statistically significant and correlated with compositional variables ($p < 0.05$; Table 4), but primarily varied along the

less explanatory PC2 (Figure 5). Areas of higher elevation produced fruit with higher concentrations of desirable components, including polymeric tannins and quercetin glycosides (Table 4).

Discussion

Remote sensing. The most significant finding of this study was the relative similarity in the relationships between fruit composition and different remote sensing platforms across multiple seasons and multiple vineyards, although relationships among many variables were not strong. Images captured from satellites, Sentinel-2 and Landsat 8 at 10-m and 30-m ground resolutions, respectively, aligned closely with those from manned aircraft at 20-cm resolution when used as predictors of fruit composition; that is, there was little, if any, benefit offered by the high-resolution airborne imagery compared to the lower resolution satellite sources. Similar studies in other regions with more diverse soil and climate variability, or in applications where higher resolution imagery is required, may be necessary to broadly extrapolate these findings. Similarly, Sozzi et al. (2020) found that Sentinel-2 images were nearly as useful as UAV imagery captured at <10 cm in describing spatial variability of canopy vigor in vineyards with no grass in the interrow, although no comparisons with fruit chemistry were reported. However, in the PCA with images captured at bloom (Figure 2A) the HR_{NDVI} was somewhat more closely related to pruning weights, unripe and green characteristics (YAN, malic acid, C6), and yield components. The results presented here expand this finding from the spatial variability noted in

Table 4 Pearson correlations accounting for spatial autocorrelation[a] between fruit composition and yield components, canopy characteristics, soil, elevation, and different sources of imagery combining measurements collected in 2018 and 2019 in the Lodi region of California.

	TSS[b] (Brix)	pH	TA[b]	Anth[b]	β-dam[b]	C6	Malic acid	IBMP[b]	Polymeric tannins	Quercetin glycosides	YAN[b]
Yield	-0.27*[c]	-0.41*	0.46*	-0.34*	-0.23*	0.20*	0.03	0.42*	-0.46*	-0.47*	0.30*
Cluster weight	-0.24*	-0.22*	0.26*	-0.26*	-0.23*	0.12*	0.03	0.33*	-0.36*	-0.35*	0.21*
Clusters	-0.16*	-0.27*	0.25*	-0.19*	-0.01	0.17*	-0.09*	0.22*	-0.28*	-0.21*	0.14*
Berry weight	-0.14*	-0.24*	0.30*	-0.40*	-0.48*	0.12*	0.01	0.36*	-0.47*	-0.33*	0.10*
Pruning weight	-0.02	0.08*	0.11*	-0.29*	-0.02	0.03	0.05	0.31*	-0.30*	-0.29*	0.25*
Ravaz index	-0.28*	-0.44*	0.29*	-0.06	-0.14*	0.18*	-0.11*	0.11*	-0.19*	-0.13*	0.02
PAR_{FZ}[d] (E-L 23)	-0.00	-0.03	0.02	0.07*	-0.04	-0.05	-0.03	0.00	0.08*	0.10*	0.00
PAR_{FZ} (E-L 27)	-0.07*	0.09*	-0.09*	0.06	0.07*	-0.08*	0.08*	-0.06	0.07*	0.19*	-0.01
PAR_{FZ} (E-L 35)	0.03	0.03	-0.10*	0.12*	0.02	-0.10*	-0.09*	-0.15*	0.11*	0.21*	-0.09*
Clay	0.01	0.05	-0.05*	-0.02	0.11*	-0.00	0.04	-0.03	0.06*	0.01	0.09*
Silt	-0.12*	-0.20*	0.18*	-0.06*	0.00	0.07*	0.04	0.11*	-0.06*	-0.08*	0.16*
Sand	0.10*	0.14*	-0.13*	0.07*	-0.06*	-0.06*	-0.04	-0.07*	0.02	0.05	-0.17*
EC_a[e]	-0.00	-0.12*	0.07*	0.08*	-0.12*	-0.00	0.12*	-0.08*	0.05	0.01	-0.01
Elevation	0.12*	0.19*	-0.16*	0.06*	0.18*	-0.17*	-0.05	-0.12*	0.22*	0.19*	0.09*
HR_{CT}[e] (E-L 23)	0.10*	0.09*	-0.16*	0.16*	-0.02	-0.11*	-0.07	-0.24*	0.25*	0.20*	-0.19*
HR_{CT} (E-L 27)	0.13*	0.20*	-0.31*	0.21*	0.12*	-0.11*	-0.10*	-0.31*	0.32*	0.36*	-0.19*
HR_{CT} (E-L 35)	0.20*	0.26*	-0.34*	0.27*	0.18*	-0.19*	0.10*	-0.43*	0.35*	0.32*	-0.24*
HR_{NDVI}[e] (E-L 23)	-0.02	0.10*	0.07*	-0.16*	-0.08*	0.14*	0.12*	0.19*	-0.21*	-0.26*	0.22*
HR_{NDVI} (E-L 27)	-0.01	-0.01	0.07*	-0.12*	-0.00	0.07*	0.08*	0.15*	-0.14*	-0.25*	0.16*
HR_{NDVI} (E-L 35)	-0.10*	-0.13*	0.24*	-0.18*	-0.10*	0.19*	0.15*	0.38*	-0.26*	-0.40*	0.28*
$S2_{NDVI}$[e] (E-L 23)	0.07*	0.08*	-0.02	-0.05*	0.05	0.09*	0.03	0.03	-0.11*	-0.10*	0.07*
$S2_{NDVI}$ (E-L 27)	0.01	-0.02	0.10*	-0.12*	-0.02	0.12*	0.06*	0.10*	-0.18*	-0.20*	0.10*
$S2_{NDVI}$ (E-L 35)	0.04	-0.05*	0.16*	-0.17*	-0.11*	0.12*	0.11*	0.19*	-0.20*	-0.26*	0.20*
$LS8_{NDVI}$[e] (E-L 23)	0.01	0.04	0.01	-0.01	-0.04	0.10*	0.07*	0.06*	-0.10*	-0.06*	0.03
$LS8_{NDVI}$ (E-L 27)	-0.01	-0.02	0.07*	-0.04	-0.08*	0.09*	0.08*	0.09*	-0.14*	-0.11*	0.04
$LS8_{NDVI}$ (E-L 35)	-0.06*	-0.07*	0.13*	-0.07*	-0.11*	0.13*	0.10*	0.15*	-0.15*	-0.17*	0.09*

[a]Modified *t*-test (Dutilleul 1993), n = 796.
[b]TSS, total soluble solids; TA, titratable acidity; Anth, anthocyanins; β-dam, β-damascenone; IBMP, 3-isobutyl-2-methoxypyrazine; YAN, yeast assimilable nitrogen.
[c]Asterisks indicate significance ($p < 0.05$).
[d]PAR_{FZ}, fruit-zone photosynthetically active radiation; modified Eichhorn-Lorenz (E-L) stages (Pearce and Coombe 2004).
[e]EC_a, apparent electrical conductivity; HR_{CT}, high-resolution canopy temperature; HR_{NDVI}, high-resolution normalized difference vegetation index; $S2_{NDVI}$, Sentinel-2 normalized difference vegetation index; $LS8_{NDVI}$, Landsat 8 normalized difference vegetation index.

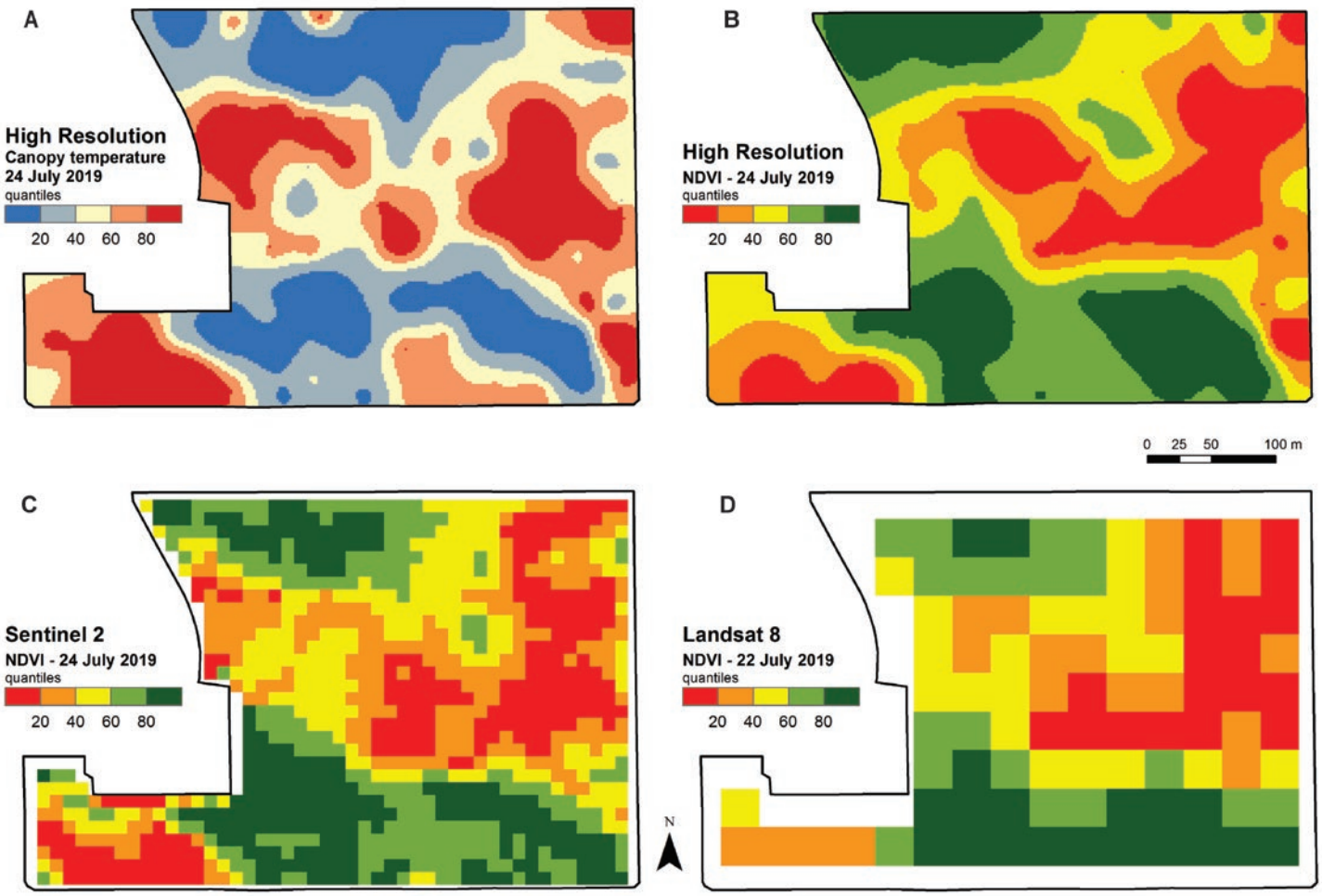

Figure 3 Spatial variation of the normalized difference vegetation index (NDVI) derived from four sources of imagery in a vineyard (Vineyard C) in the Lodi region of California at veraison (modified Eichhorn-Lorenz [E-L] stage 35 [Pearce and Coombe 2004]) in 2019 showing (**A**) high-resolution canopy temperature (HR_{CT}), (**B**) high-resolution NDVI (HR_{NDVI}), (**C**) Sentinel-2 NDVI ($S2_{NDVI}$), and (**D**) Landsat 8 NDVI ($LS8_{NDVI}$). Note that the map data have been classified as quantiles (20th percentiles).

several fruit compositional parameters (Sams et al. 2022). There may be applications or time sensitive phenological stages where canopy separation from the interrow is imperative for determining vine water status, where an absolute value is necessary to calibrate with ground data, or in vineyards with native, nontilled vegetation occurring in irregular patches, but our results show that this separation may be unnecessary to describe spatial variability of vineyard canopies. Possible explanations for this scenario are that areas comprised of low vigor vines will also cause low vigor of the interrow cover crop, or that by the time of image acquisition at these phenological stages, the interrow cover crop is dead or dormant and provides a mostly bare background. It could be possible that a combination of these two explanations may actually enhance visual patterns of variability because low vigor zones contain more interrow space with soil or dead vegetation as a percentage of ground cover. The separation of nonvine signal from vine canopy is not trivial because image processing represents significant economic cost to imagery providers who then pass this on to customers. Furthermore, a major benefit of the satellite data examined here is the high-level calibration made by those providing the imagery (NASA and ESA), although given the weak correlations between imagery values and fruit composition, viticulturists may be more interested in spatial patterns found in imagery because absolute values from vegetation indices may vary over multiple images. When compared with maps of fruit composition in these same vineyards shown by Sams et al. (2022), this finding of pattern importance may be even more relevant. With this in mind, growers interested in assessing variability of vineyards may still be better suited to use lower-resolution, publicly available imagery at no cost, rather than purchase higher resolution from vendors because the relationships between imagery and fruit composition described here were not sufficiently strong to give absolute predictive value. For more precise prediction of fruit composition from remote sensing, it is likely that alternatives such as hyperspectral imagery at high resolution may be needed, although neither the precision nor cost-effectiveness of such an approach is known at present.

Similar to our results, Carrillo et al. (2016) found that berry weight, cluster number, and NDVI were similarly aligned

along the first principal component in a similar use of PCA. Ballesteros et al. (2020) used NDVI (with other indices) from an unmanned aerial sensor and machine learning techniques to model grapevine yield in *Vitis vinifera* cv. Bobal, but found contrasting results to those presented here. The authors stated that the soil background was the primary cause for a negative relationship between yield and NDVI when inter-row and shadow pixels were included in the analysis, but when those pixels were removed, the relationship was positive immediately prior to harvest. These authors made a similar recommendation to ours, in that seasonal calibration is likely necessary for the most accurate results.

Environmental conditions and fruit composition. Differences in growing degree days, incoming solar radiation, precipitation, and reference evapotranspiration were likely partly responsible for differences in fruit composition among

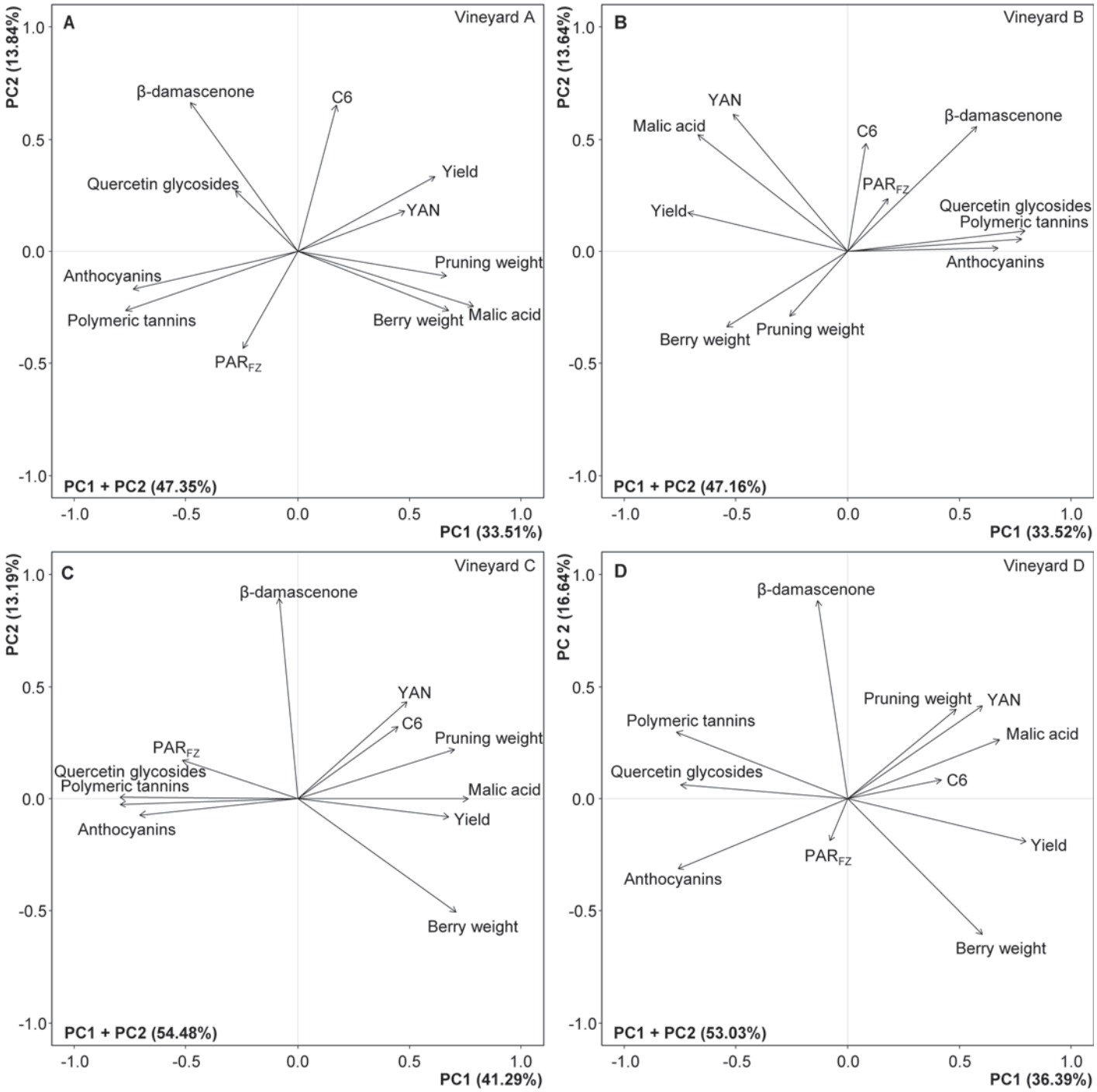

Figure 4 Principal component analysis (PCA) of fruit components (anthocyanins, β-damascenone, C6, malic acid, polymeric tannins, quercetin glycosides, and yeast assimilable nitrogen [YAN]), yield components (total vine yield and average berry weight by vine), and canopy characteristics (fruit-zone photosynthetically active radiation [PAR_{FZ}] and pruning weights) measured in 2018 and 2019 in four vineyards in the Lodi region of California and standardized by season (μ = 0, σ = 1), (**A**) Vineyard A, (**B**) Vineyard B, (**C**) Vineyard C, and (**D**) Vineyard D. n = 250.

the three years of study (Table 1). In 2018, dormant season precipitation (leaf fall to budbreak) was much lower than in the other dormant seasons. This difference, coupled with the slower accumulation of growing degree days in 2018 and higher incoming radiation (Table 1), may explain the large increase in anthocyanin concentration in all four vineyards from 2017 to 2018 (Van Leeuwen et al. 2009; Table 3). However, quercetin glycosides and polymeric tannins were lowest in 2018 in all four vineyards, marking a separation in development between anthocyanins and these phenolic compounds during these seasons, despite the consistent grouping apparent in Figures 2, 4, and 5. Despite the relatively cooler season, a lack of precipitation in the early season (Table 1), and only small differences in irrigation volume (Table 2), yield was also highest in 2018 in all four vineyards (Table 3).

While a case can be made that lower yield equates to an increase in some positive aspects of fruit composition, the reasons for this relationship are somewhat misunderstood (Smart and Robinson 1991). In many cases, low-yielding vines often have small canopies and leaf areas but higher PAR_{FZ}, allowing more light into the canopy interior than a vine with identical yield, larger canopies, and lower PAR_{FZ}. Previous studies have linked light interception with fruit composition in California (e.g., Bergquist et al. 2001, Kliewer and Dokoozlian 2005), and their results complement those presented in this study. Low PAR_{FZ} was likely at least partly responsible for the relatively low values of anthocyanins, polymeric tannins, and anthocyanins in Vineyard A. Extremely high (or low) vigor may affect measurements of light interception through excessive sensor occlusion (or through direct sensor exposure in the case of low vigor). The values of IBMP and C6 are likely elevated in this vineyard due to excessive shading in the fruit zone. Given the low percentage of ambient PAR reaching the fruit zone, large clusters, and relatively high crop load on a single bilateral cordon (Tables 2 and 3), cluster occlusion may also be responsible for these results in Vineyard A (Dunn and Martin 2004). Leaf area can vary greatly between different canopy architectures, and many cultural manipulations are difficult to detect from remote sensing. Trellis design, pruning, leaf removal, irrigation, and crop load management are all parts of this complex system and contribute greatly to the decision-making process as well as to the cost of vineyard management (Jackson and Lombard 1993 and references within).

The relatively weak results from analyses of soil and topographic variables may be related to the way in which they were sampled but may also stem from the adjustment of management practices such as canopy management and irrigation, based on the highly variable soils, which can directly or indirectly influence canopy light interception (Table 4). It may also be possible that the magnitude of variability in soil and topography were insufficient to cause large differences in these vineyards and may differ in other regions or conditions. Shallow soil profiles on slopes and hillsides can produce differences in water holding capacity and lead to smaller vines compared with those on foothills or flat surfaces (Van Leeuwen et al. 2004, Jasse et al. 2021). It also may be responsible for the relationships between elevation, yield, and fruit composition (Figure 5), although soil horizon depths were not measured in this study. Additionally, inherent spatial variability of soil can cause drastic differences in yield and fruit quality, even over short distances, or small changes in topography (Bramley and Hamilton 2004, Bramley 2005); results presented in this study also suggest that elevation and soil texture have a significant effect on many aspects of fruit composition (Table 4). Accordingly, a more detailed investigation using measurements made down the soil profile and using a survey-grade GPS for elevation may lead to more precise understanding of soil and terrain effects.

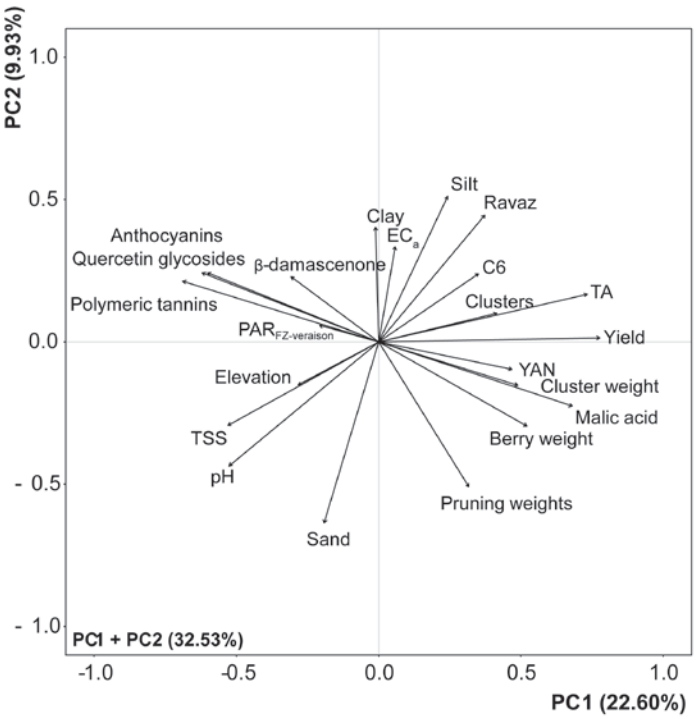

Figure 5 Principal component analysis (PCA) of fruit components (anthocyanins, β-damascenone, C6, malic acid, pH, polymeric tannins, quercetin glycosides, titratable acidity [TA], total soluble solids [TSS], and yeast assimilable nitrogen [YAN]), yield components (total vine yield, average cluster weight by vine, cluster number per vine, and average berry weight by vine), canopy characteristics (fruit-zone photosynthetically active radiation [PAR_{FZ}], pruning weights, and Ravaz index), soil texture (clay, sand, and silt), apparent electrical conductivity (EC_a), and elevation data measured in 2018 and 2019 from four vineyards (A, B, C, and D) in the Lodi region of California, aggregated and standardized ($\mu = 0$, $\sigma = 1$) by vineyard and season. n = 1000.

The combination of high-density fruit composition samples and related vineyard measurements from several large commercial vineyards presented in this study can act as a guide to the industry as to which indirect or destructive measurements are truly useful in describing and predicting fruit composition. Targeted PAR measurements, pruning weights, and/or yield estimates collected from spatially distinct "quality" zones like those shown by Sams et al. (2022), compared with a few fruit composition samples taken with these zones in mind, should provide growers and wineries with a guide to the potential quality variability in a vineyard.

Conclusion

This study illustrates that remote sensing data from low resolution satellites paired with spatially targeted seasonal calibrations of yield components, pruning weights, and/or fruit composition can describe relationships between fruit composition and vegetative vigor at relatively low cost with sufficient precision to support delineation of within-vineyard zones of different vineyard performance, although additional studies may be necessary in different regions or in different conditions. If calibrations are conducted among different growing conditions and specific cultural and management practices (e.g., trellising, canopy management, water status), it should eventually be possible to model these systems with high precision and accuracy with minimal ground validation. As satellite imagery becomes more widely available and spatial and temporal resolution increases, growers will have even more options available to tailor vineyard management to specific production targets. Data products developed from these sensors, such as estimates of crop evapotranspiration or leaf area index, will also become more useful for more applications such as yield prediction, irrigation management, and environmental damage assessment. The current study may be useful to growers for reducing the costs of acquiring information about how variability affects the magnitude of fruit quality differences in vineyards. Until handheld, proximal sensors capable of detecting fruit composition are readily available at costs suitable for commercial growers and wineries, remote sensing products provide the best platform for capturing this information.

Literature Cited

Acevedo-Opazo C, Tisseyre B, Guillaume S and Ojeda H. 2008. The potential of high-resolution information to define within-vineyard zones related to vine water status. Precis Ag 9:285-302.

Arnó J, Rosell JR, Blanco R, Ramos MC and Martínez-Casasnovas JA. 2012. Spatial variability in grape yield and quality influenced by soil and crop nutrition characteristics. Precis Ag 13:393-410.

Ballesteros R, Intrigliolo DS, Ortega JF, Ramírez-Cuesta JM, Buesa I and Moreno MA. 2020. Vineyard yield estimation by combined remote sensing, computer vision and artificial neural network techniques. Precis Ag 21:1242-1262.

Bergqvist J, Dokoozlian NK and Ebisuda N. 2001. Sunlight exposure and temperature effects on berry growth and composition of Cabernet Sauvignon and Grenache in the Central San Joaquin Valley of California. Am J Enol Vitic 52:1-7.

Bramley RGV. 2005. Understanding variability in winegrape production systems 2. Within vineyard variation in quality over several vintages. Aust J Grape Wine Res 11:33-42.

Bramley RGV and Hamilton RP. 2004. Understanding variability in winegrape production systems 1. Within vineyard variation in yield over several vintages. Aust J Grape Wine Res 10:32-45.

Bramley RGV, Ouzman J and Boss P. 2011. Variation in vine vigour, grape yield and vineyard soils and topography as indicators of variation in the chemical composition of grapes, wine and wine sensory attributes. Aust J Grape Wine Res 17:217-229.

Canuti V, Conversano M, Calzi ML, Heymann H, Matthews MA and Ebeler SE. 2009. Headspace solid-phase microextraction–gas chromatography-mass spectrometry for profiling free volatile compounds in Cabernet Sauvignon grapes and wines. J Chromatogr A 1216:3012-3022.

Carrillo E, Matese A, Rousseau J and Tisseyre B. 2016. Use of multispectral airborne imagery to improve yield sampling in viticulture. Precis Ag 17:74-92.

Dobrowski SZ, Ustin SL and Wolpert JA. 2002. Remote estimation of vine canopy density in vertically shoot-positioned vineyards: determining optimal vegetation indices. Aust J Grape Wine Res 8:117-125.

Dunn GM and Martin SR. 2004. Yield prediction from digital image analysis: a technique with potential for vineyard assessments prior to harvest. Aust J Grape Wine Res 10:196-198.

Dutilleul P. 1993. Modifying the t test for assessing the correlation between two spatial processes. Biometrics 49:305-314.

Ferreira CSS, Veiga A, Caetano A, Gonzalez-Pelayo O, Karine-Boulet A, Abrantes N, Keizer J and Ferreira AJD. 2020. Assessment of the impact of distinct vineyard management practices on soil physicochemical properties. Air, Soil and Water Res 13:1-13.

Gesch DB, Oimoen MJ and Evans GA. 2014. Accuracy assessment of the U.S. Geological Survey National Elevation Dataset, and comparison with other large-area elevation datasets–SRTM and ASTER: U.S. Geological Survey Open-File Report 2014-1008.

Gladstones J. 1992. Viticulture and Environment. Winetitles, Adelaide.

Gorelick N, Hancher M, Dixon M, Ilyushchenko S, Thau D and Moore R. 2017. Google Earth Engine: Planetary-scale geospatial analysis for everyone. Remote Sens Environ 202:18-27.

Hall A, Lamb DW, Holzapfel BP and Louis JP. 2011. Within-season temporal variation in correlations between vineyard canopy and winegrape composition and yield. Precis Ag 12:103-117.

Ibarz MJ, Ferreira V, Hernández-Orte P, Loscos N and Cacho J. 2006. Optimization and evaluation of a procedure for the gas chromatographic-mass spectrometric analysis of the aromas generated by fast acid hydrolysis of flavor precursors extracted from grapes. J Chromatogr A 1116:217-229.

Iland P, Ewart A, Sitters J, Markides A and Bruer N. 2000. Techniques for chemical analysis and quality monitoring during winemaking. Patrick Iland Wine Promotions, Campbelltown.

Jackson DI and Lombard PB. 1993. Environmental and management practices affecting grape composition and wine quality-a review. Am J Enol Vitic 44:409-430.

Jasse A, Berry A, Aleixandre-Tudo JL and Poblete-Echeverría C. 2021. Intra-block spatial and temporal variability of plant water status and its effect on grape and wine parameters. Agr Water Manage 246:1006696.

Johnson LF. 2003. Temporal stability of an NDVI-LAI relationship in a Napa Valley vineyard. Aust J Grape Wine Res 9:96-101.

Keller M, Mills LJ, Wample RL and Spayd SE. 2005. Cluster thinning effects on three deficit-irrigated Vitis vinifera cultivars. Am J Enol Vitic 56:91-103.

Kliewer WM and Dokoozlian NK. 2005. Leaf area/crop weight ratios of grapevines: influence on fruit composition and wine quality. Am J Enol Vitic 56:170-181.

Kotseridis Y, Baumes RL and Skouroumounis GK. 1999. Quantitative determination of free and hydrolytically liberated beta-damascenone in red grapes and wines using a stable isotope dilution assay. J Chromatogr A 849:245-254.

Kotseridis YS, Spink M, Brindle ID, Blake AJ, Sears M, Chen X, Soleas G, Inglis D and Pickering GJ. 2008. Quantitative analysis of 3-alkyl-2-methoxypyrazines in juice and wine using stable isotope-labeled internal standard assay. J Chromatogr A 1190:294-301.

Lamb DW, Weedon MM and Bramley RGV. 2004. Using remote sensing to predict grape phenolics and colour at harvest in a Cabernet Sauvignon vineyard: Timing observations against vine phenology and optimising image resolution. Aust J Grape Wine Res 10:46-54.

Lê S, Josse J and Husson F. 2008. FactoMineR: a package for multivariate analysis. J Stat Software 25:1-18.

Lee SH, Seo MJ, Riu M, Cotta JP, Block DE, Dokoozlian NK and Ebeler SE. 2007. Vine microclimate and norisoprenoid concentration in Cabernet Sauvignon grapes and wines. Am J Enol Vitic 58:291-301.

Li JH, Guan L, Fan PG, Li SH and Wu BH. 2013. Effect of sunlight exclusion at different phenological stages on anthocyanin accumulation in red grape clusters. Am J Enol Vitic 64:349-356.

Martínez-Lüscher J, Brillante L and Kurtural SK. 2019. Flavonol profile is a reliable indicator to assess canopy architecture and the exposure of red wine grapes to solar radiation. Front Plant Sci 10:10.

Meyers JM, Sacks GL, Van Es HM and Vanden Heuvel JE. 2011. Improving vineyard sampling efficiency via dynamic spatially explicit optimization. Aust J Grape Wine Res 17:306-315.

Niimi J, Tomic O, Næs T, Bastian SEP, Jeffrey DW, Nicholson EL, Maffei SM and Boss PK. 2020. Objective measures of grape quality: from Cabernet Sauvignon grape composition to wine sensory characteristics. LWT—Food Sci Technol 123:109105.

Pearce I and Coombe BG. 2004. Grapevine phenology. *In* Viticulture 1–Resources 2nd edition. Dry P and Coombe BG (eds.), p. 153. Winetitles, Adelaide.

Peng Z, Hayasaka Y, Iland PG, Sefton M, Høj P and Waters EJ. 2001. Quantitative analysis of polymeric procyanidins (tannins) from grape (Vitis vinifera) seeds by reverse phase high-performance liquid chromatography. J Agric Food Chem 49:26-31.

Reynolds AG, Taylor G and de Savigny C. 2013. Defining Niagara terroir by chemical and sensory analysis of Chardonnay wines from various soil textures and vine sizes. Am J Enol Vitic 64:180-194.

Rouse JW, Haas RH, Schell JA and Deering DW. 1974. Monitoring vegetation systems in the Great Plains with ERTS. *In* Goddard Space Flight Center 3rd ERTS Symposium, pp. 309-317. NASA.

Salgadoe ASA, Robson AJ, Lamb DW and Schneider D. 2019. A non-reference temperature histogram method for determining Tc from ground-based thermal imagery of orchard tree canopies. Remote Sensing 11:714.

Sams B, Bramley RGV, Sanchez LA, Dokoozlian NK, Ford CM and Pagay VV. 2022. Characterising spatio-temporal variation in fruit composition for improved winegrowing management in California Cabernet Sauvignon. Aust J Grape Wine Res https://doi.org/10.1111/ajgw.12542 [Early View].

Smart RE and Robinson MD. 1991. Sunlight into Wine: A Handbook for Winegrape Canopy Management. Winetitles, Adelaide.

Song J, Smart RE, Dambergs RG, Sparrow AM, Wells RB, Wang H and Qian MC. 2014. Pinot Noir wine composition from different vine vigour zones classified by remote imaging technology. Food Chem 153:52-59.

Sozzi M, Kayad A, Marinello F, Taylor J and Tisseyre B. 2020. Comparing vineyard imagery acquired from Sentinel-2 and Unmanned Aerial Vehicle (UAV) platform. OENO One 54:189-97.

Sun L et al. 2017. Daily mapping of 30 m LAI and NDVI for grape yield prediction in California vineyards. Remote Sensing 9:317.

Trought MCT and Bramley RGV. 2011. Vineyard variability in Marlborough, New Zealand: characterising spatial and temporal changes in fruit composition and juice quality in the vineyard. Aust J Grape Wine Res 17:79-89.

Vallejos R, Osorio F and Bevilacqua M. 2020. Spatial relationships between two georeferenced variables: with applications in R. Springer, New York.

Van Leeuwen C, Friant P, Choné X, Tregoat O, Koundouras S and Dubourdieu D. 2004. Influence of climate, soil, and cultivar on terroir. Am J Enol Vitic 55:207-217.

Van Leeuwen C, Tregoat O, Choné X, Bois B, Pernet P and Gaudillère JP. 2009. Vine water status is a key factor in grape ripening and vintage quality for red Bordeaux wine. How can it be assessed for vineyard management purposes? OENO One 43:121-134.

Vermote E, Justice C, Claverie M and Franch B. 2016. Preliminary analysis of the performance of the Landsat 8/OLI land surface reflectance product. Rem Sen Envmt. 185:46-56.

Whiton R and Zoecklein B. 2002. Evaluation of glycosyl-glucose analytical methods for various glycosides. Am J Enol Vitic 53:315-317.

Wolpert JA and Vilas EP. 1992. Estimating vineyard yields: introduction to a simple, two step method. Am J Enol Vitic 43:384-388.